Article

J. Mex. Chem. Soc. **2008**, *52(1)*, 54-59

ISSN 1870-249X

Synthesis, Structure and Magnetic Differences of Two α-Nitronyl Nitroxide Isomers

Araceli Vega, [1] Juan Padilla,*[1] Marco Antonio Leyva,[2] María del Jesús Rosales,[2] and Sylvain Bernès[3]

[1] Departamento de Química, Universidad Autónoma Metropolitana Iztapalapa, Av. R. Atlixco 186, Col. Vicentina, R-116. Tel.: (55)5804-4678. Fax: (55)5804-4666. E-mail: jpn@xanum.uam.mx
[2] Departamento de Química, Centro de Investigaciones y Estudios Avanzados, Apartado Postal 14-740. México, D.F.
[3] DEP, Facultad de Ciencias Químicas, UANL, Guerrero y Progreso S/N, Col. Treviño, 64570 Monterrey, N. L., México

Recibido el 30 de septiembre del 2007; aceptado el 14 de febrero del 2008

Abstract. The two isomeric organic nitronyl nitroxide free radicals 2-(2'-hydroxyl-3'-methoxy-phenyl)-4, 4, 5, 5-tetramethyl-4, 5-dihydro-1H-imidazoyl-1-oxyl-3-oxide, **1**, and 2-(3'-hydroxyl-4'-methoxy-phenyl)-4, 4, 5, 5-tetramethyl-4, 5-dihydro-1H-imidazoyl-1-oxyl-3-oxide, **2**, have been synthesized and their structures determined by X-ray diffraction. Structure **1** has three dimensional, strong, intramolecular hydrogen bonds in addition to intermolecular interactions favoring sheets. The structure of radical **2** also shows strong hydrogen bonds both intra- and intermolecular. Some of these bonds are with a lattice water molecule, yielding a three-dimensional crystal structure. An important structural difference between both radicals is that in compound **1**, one of the nitrogen atoms of the radical shows smaller angles than the other atom in the same radical and than both nitrogen atoms in compound **2**. This suggests that in **1**, one of the nitrogen atoms has a higher sp^3 character than the other. This proposal is supported by the N-O bond length which is significantly longer in the sp^3 nitrogen side. Both isomers show quite different magnetic behavior. In **1** there are both ferromagnetic (J_F/k = + 0.11 ± 0.01 K) and antiferromagnetic (J_{AF}/k = - 0.81 ± 0.10 K) interactions, whereas **2** only shows antiferromagnetism (J_{AF}/k = - 1.60 ± 0.02 K) with a phase transition at T_c = 2.48 K.
Key words: Organic radicals, isomers, nitronyl nitroxides, ferromagnetism, antiferromagnetism, phase transition, structure.

Resumen. Se sintetizaron y determinaron las estructuras cristalinas por difracción de rayos-X de dos isómeros de radicales orgánicos libres nitronilo nitróxido: el 2-(2'-hidroxilo-3'-metoxilo-fenilo)-4, 4, 5, 5-tetrametilo-4, 5-dihidro-1H-imidazoilo-1-oxilo-3-óxido, **1**, y el 2-(3'-hidroxilo-4'-metoxilo-fenilo)-4, 4, 5, 5-tetrametilo-4, 5-dihidro-1H-imidazoilo-1-oxilo-3-óxido, **2**. La estructura **1** presenta un enlace de hidrógeno intramolecular fuerte en un arreglo tridimensional, aunque también se observan interacciones intermoleculares que favorecen la formación de láminas. La estructura del radical **2** también muestra puentes de hidrógeno tanto intra- como intermoleculares. Algunos de estos enlaces son con una molécula de agua de cristalización, dando lugar a una estructura tridimensional. Una diferencia estructural importante entre ambos radicales es que en el compuesto **1**, uno de los átomos de nitrógeno del radical muestra ángulos más pequeños que el otro átomo de nitrógeno en el mismo radical y que ambos átomos de nitrógeno en el compuesto **2**. Esto sugiere que en **1**, uno de los átomos de nitrógeno tiene un mayor carácter sp^3 que el otro. Esta propuesta es apoyada también por la distancia de enlace N-O que es significativamente más larga en el lado del nitrógeno sp^3. El comportamiento magnético de ambos isómeros es muy diferente, mientras que en **1** están presentes tanto interacciones ferromagnéticas (J_F/k = + 0.11 ± 0.01 K) como antiferromagnéticas (J_{AF}/k = - 0.81 ± 0.10 K), el radical **2** solo se comporta antiferromagnéticamente (J_{AF}/k = - 1.60 ± 0.02 K) con una transición de fase a T_c = 2.48 K.
Palabras clave: Radicales orgánicos, isómeros, nitronilo nitróxidos, ferromagnetismo, antiferromagnetismo, transición de fase, estructura.

Introduction

The field of organic molecular magnetism had a quick development after the discovery for the first time of a purely organic ferromagnet [1], starting the synthesis of molecules with a variety of magnetic behaviors such as ferro- antiferro- and ferrimagnetism, in particular of the stable organic free radicals nitronyl nitroxides. Of paramount importance in the three dimensional arrangement of the crystalline lattice is the presence of hydrogen bonds [2], considered a driving force in the synthesis of radicals, where one of the most common examples are the hydroxyphenyl nitronyl nitroxides [3-6] with their magnetic behavior directly influenced by the position of the substituents in the aromatic ring. In order to characterize the magnetic phase transition, heat capacity measurements are best to determine the transition temperature [1, 7-12] although it usually occurs at temperatures lower than 1 K, with exception of radical F_5PNN with a transition near 2 K [13-15]. Here we report a T_c = 2.48 K for radical **2**.

Results and Discussion

The molecular geometry of radicals **1** and **2** are shown in Figures 1 and 2, respectively, with some selected bond lengths and angles, and Table 1 summarizes some crystallographic data.

The structures of compounds **1** and **2** show slightly different conformations; the angle between the NCN plane and the aromatic ring is 29.16º in **1** and 32.22º in **2**. However it must be pointed out that the five-membered ring is almost planar in compound **2** (C(9) deviates 0.218 Å and C(10) 0.055 Å from the NCN plane), while the same ring is more distorted in compound **1** (C(9) deviates 0.498 Å and C(10) 0.070 Å from the NCN plane). Obviously, this difference is a direct consequence of the strong intramolecular hydrogen bond in **1**, not present in **2** due to the position of the OH group. Torsion angles within the ring reflect the distortion since in radical **1** absolute values range from 3.0 to 33.19º while in radical **2** span the range from 2 to 16º with three of these values below 10º.

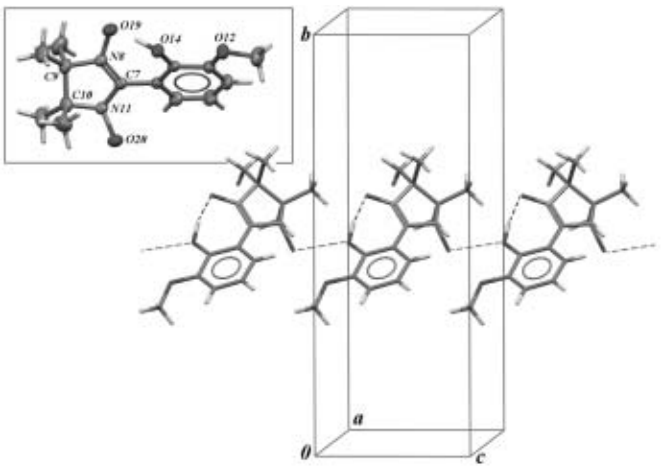

Fig. 1. X-ray molecular (inset) and crystal (main figure) structures for radical **1**. Some selected bond lengths and angles are: N(8)-O(19) 1.336(2) Å, N(11)-O(20) 1.422(2) Å, C(7)-N(8) 1.302(2) Å, C(7)-N(11) 1.385(2) Å, N(8)-C(9) 1.479(3), C(10)-N(11) 1.503(3) Å; C(7)-N(8)-O(19) 126.16(16)º, C(7)-N(8)-C(9) 112.86(16)º, O(19)-N(8)-C(9) 118.60(15)º, C(7)-N(11)-O(20) 113.04(14)º, C(7)-N(11)-C(10) 106.82(15)º, O(20)-N(11)-C(10) 114.08(16)º. Dashed lines represent hydrogen bonds and O...O contacts involved in the crystal structure.

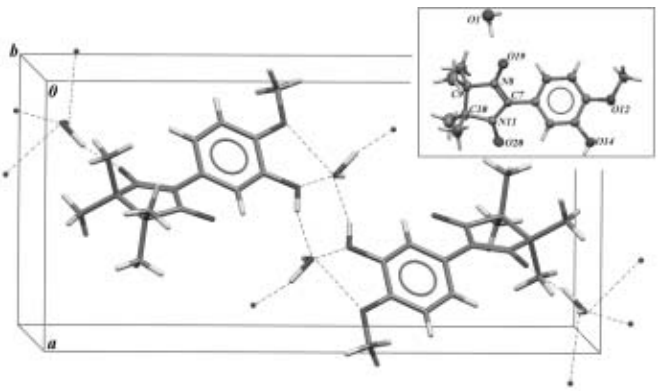

Fig. 2. X-ray molecular (inset) and crystal (main figure) structures for radical **2**. Some selected bond lengths and angles are: O(20)-N(11) 1.275(3)Å, O(19)-N(8) 1.291(3)Å, C(7)-N(11) 1.351(4) Å, C(7)-N(8) 1.341(4) Å, C(9)-N(8) 1.495(4) Å, C(10)-N(11) 1.506(4) Å; C(7)-N(11)-C(10) 112.7(2)º, C(7)-N(11)-O(20) 125.6(3)º, C(10)-N(11)-O(20) 121.7(2) º, C(7)-N(8)-C(9) 113.6(2)º, C(7)-N(8)-O(19) 125.2(3) º, C(9)-N(8)-O(19) 121.1(2)º. Dashed lines represent hydrogen bonds and O...O contacts involved in the crystal structure.

Table 1. Crystallographic data for radicals **1** and **2**.

	1	**2**
Empirical formula	$C_{14}H_{19}N_2O_4$	$C_{14}H_{21}N_2O_5$
Formula weight (g/mol)	279.31	297.33
Crystal size (mm)	0.70 × 0.36 x 0.22	0.42 × 0 .2 × 0.1
Crystal colour	Dark brown	Dark blue flakes
Crystal system	Tetragonal	Orthorhombic
Space group	$P4_2/n$	*Pbca*
Unir cell dim. *a*, *b*, *c* (Å).	*a* = 20.0640(8), *b* = 20.0640(8), *c* = 7.3819(5)	*a* = 9.7555(3), *b* = 15.4585(4), *c* = 20.0796(6)
Volume ($Å^3$)	2971.7(3)	3028.11(15)
Z	8	8
Density (calc.) (Mg/m^3)	1.249	1.304
Absorption Coefficient (mm^{-1})	0.092	0.099
F(000)	1192	1272
Diffractometer used	Siemens P4	Nonius Kappa CCD
Radiation and wavelength	MoKα with λ = 0.71073 Å	MoKα with λ = 0.71073 Å
Scan type	ω-θ	ω-ϕ
Temperature (K)	293	293
2θ range for collection	4.06 to 52º	7.02 to 52.04°
Index ranges	-1 ≤ h ≤ 24; -24 ≤ k ≤ 1; -9 ≤ l ≤ 9	-10 ≤ h ≤ 10; -18 ≤ k ≤ 19; -24 ≤ l ≤ 24
Reflections collected	6664	5370
Independent reflections	2929 (R_{int} = 0.0293)	2893 (R_{int} = 0.0390)
Observed reflections	1974	1435 (F> 3σ (F))
Final R indices [F>nσ(F)]	R1 = 0.0479, wR2 = 0.1270, *n* = 2	R1 = 0.0444, wR2 = 0.0536, *n* = 3
R indices (all data)	R1 = 0.0762, wR2 = 0.1426	R1 = 0.1057, wR2 = 0.1054
GOOF on F^2	1.022	0.8419
Max, min peaks, $eÅ^{-3}$	0.384, -0.185	0.32 , -0.19

The ring distortion in radical **1** must be related to the bond angles observed within the ring, in particular about the nitrogen atoms. While in radical **2**, angles C(7)-N(11)-C(10) and C(7)-N(8)-C(9) are 112.7(2)º and 113.6(2)º respectively, whereas the remaining angles around the N(11) and N(8) atoms are 125.6(3)º, 121.7(2)º, 125.2(3)º and 121.1(2)º respectively. In radical **1**, the corresponding angles around N(11) are much smaller, with values of 106.82(15)º (internal), 113.04(14)º and 114.08(16)º. N(8) in radical **1** presents values similar to those observed in radical **2**. These values can be explained by proposing that N(11) in **1** has a larger sp^3 character than N(8). In radical **1** the N(11)-O(20) bond, (1.422(2)Å) is significantly longer than N(8)-O(19) [1.336(2) Å]. The corresponding bond lengths in radical **2** (1.275(3) and 1.291(3) Å), are even shorter. A longer N(11)-O(20) distance would be consistent with a larger sp^3 character for N(11). Values for the N-O distance in this type of compounds have been reported to range from 1.258(2) to 1.303(2) Å [10, 16-17]. To the best of our knowledge, this is the first case in the family of nitronyl nitroxide radicals where the two nitrogen atoms on the same radical have such a difference on the hybridization character.

In the crystal packing of radical **1**, an interplanar separation between average planes of parallel benzene rings of 8.596 Å is observed, the separation between centroids of the five member ring and the benzene ring are 9.144 Å apart, and it shows a strong intramolecular hydrogen bond (H_{14}...O_{19}, 1.43(3) Å; O_{14}–H_{14}...O_{19}, 163(3)º) allowed by the hydroxy *ortho* substitution of the benzene ring. In addition, intermolecular contacts link molecules into chains (O_{14}···O_{20}, 2.764 Å; N_{11}–O_{20}...O_{14}, 105.62º), the O...O separation being smaller than the van der Waals radii sum (O: 1.52 Å). A 3D framework is formed through further weak interactions (Fig. 3) which provide paths for superexchange magnetic interactions (*vide infra*).

In the case of radical **2**, there is a lattice water molecule, O(1), in the packing arrangement, and this participates in the formation of hydrogen bonds (H_{14}...O_1, 1.848 Å; O_{14}...H_{14}...O_1, 159.72º; O_{14}...O_1, 2.677 Å; and also H_{1B}...O_{19}, 1.650 Å; O_1...H_{1B}...O_{19}, 165.33º; O_1...O_{19}, 2.707 Å) while the hydrogen atoms of the water molecule bond to O(12) and O(14) (ether and hydroxyl) groups of *different* radical molecules yielding a three-dimensional network (Fig. 4).

Magnetic Properties

The EPR spectra at room temperature in polycrystalline powders for radicals **1** and **2** show sharp peaks at g = 2.0069 and 2.0075, and peak-to-peak bandwidths ΔH_{pp} = 11.77 and 10.64, respectively, without significant spin-orbit coupling, indicative of the radical nature of the species (Fig. 5); although radical **1** shows a splitting of the main signal due to inequivalent nitrogens (one has more sp^3 character than the other).

Also, the EPR spectra were measured in three different solvents of different polarity: water, dichloromethane and benzene at room temperature and 77 K. At room temperature the spectra show five signals, indicative of hyperfine splitting with the free electron delocalized in the fragment O-N-C-N-O. The hyperfine parameter a increases as the polarity increases (Table 2) because a more polar solvent causes an increased spin density on the nitrogen atom and a stronger interaction between the free electron and the nitrogen nucleus. The EPR spectra were simulated in solution with the software Simfonia.®

The magnetic susceptibility data were corrected for diamagnetism using Pascal's constants: $\chi_D = -160 \times 10^{-6}$ emu/mol for radical **1**, and $\chi_D = -173 \times 10^{-6}$ emu/mol for radical **2**. As can be seen in Fig. 6, χT for radical **1** decreases as the temperature goes down in a linear fashion, and the $1/\chi$ plot deviates substantially from linearity, suggesting the co-existence of both ferro- and antiferromagnetic interactions compensating each other but predominating the latter. A possible mechanism is the ferromagnetic coupling via the hydrogen bonds through the -N-O···H-O between neighbor molecules due to spin polarization on one side, and the coupling through short contacts in -N-O···O-N along the chain yielding antiferromagnetic interactions on the other [18-19]. The susceptibility data for radical **1** was fitted with a Heisenberg chain Hamiltonian of S = ½ spins with alternating ferromagnetic (F) and antiferromagnetic (AF) intermolecular exchange interactions [6, 20].

$$H = -\sum [(J_{AF} S_{2i} S_{2i+1}) + (J_F S_{2i} S_{2i-1})]$$

$$\chi T = T [(AT^3 + BT^2 + CT + D) / (T^4 + ET^3 + FT^2 + GT + H)] / \{1 - 2zJ' [(AT^3 + BT^2 + CT + D) / (T^4 + ET^3 FT^2 + GT + H)] / Ng^2\beta^2]\}.$$

zJ' = intermolecular exchange interaction.

The parameters A to H are adjusted to a polynomial function [19]:

$$X = x_0 + x_1\alpha + x_2\alpha^2 + x_3\alpha^3.$$

α = ferromagnetic/antiferromagnetic alternating parameter.

The fitting to the model yields J_{AF}/k = -0.81 ± 0.10 K, J_F/k = + 0.11 ± 0.01 K, zJ' = 0.013 K and g = 2.0067 ± 0.0002. The absence of a broad maximum in Fig. 6 indicates that the antiferromagnetic interaction predominates as confirmed by the fitting [6].

As a contrast, radical **2** obeys the Curie-Weiss law with the Curie constant C = 0.350 ± 0.007 emu mol^{-1} K, and the Weiss constant θ = - 3.66 ± 0.70 K. The χT *vs.* T curve shows the characteristic behavior expected for an antiferromagnet (Fig. 7). The magnetic susceptibility data was fitted to a Heisenberg model for an antiferromagnetic S = 1/2 chain [21] yielding J_{AF}/k = -1.60 ± 0.02 K, and g = 2.0061 ± 0.0002.

$$\chi = (Ng^2\beta^2/kT)(0.25+0.074975\, x + 0.075235\, x^2 / 1+0.9931\, x + 0.172135\, x^2 + 0.757825\, x^3).$$

Where $x = |J| / k\, T$

The crystal packing shows along the chains two contacts between the aromatic ring and the methyl groups of the imidazol ring that provides an antiferromagnetic path.

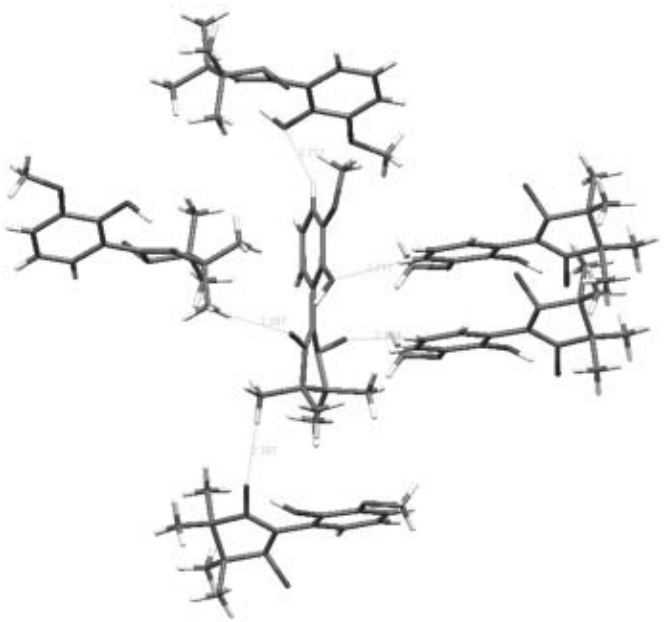

Fig. 3. The extended structure of radical **1** showing the interactions that lead to potential paths for magnetic ordering.

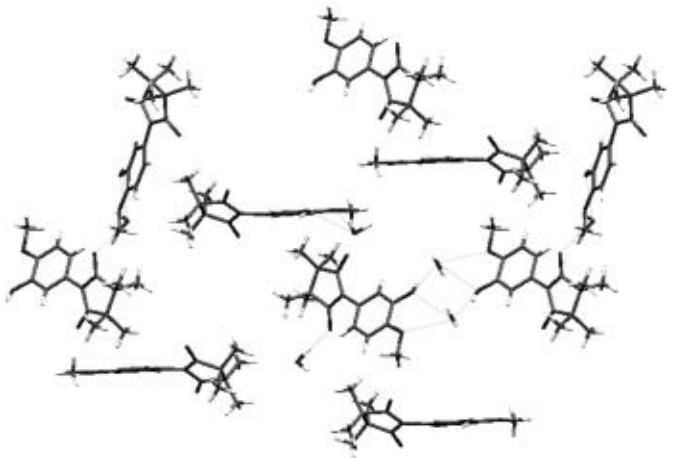

Fig. 4. Three-dimensional hydrogen bonding network on radical **2**.

At low temperatures, radical **2** shows a hump, which is reproduced in the heat capacity measurements (Fig. 8), indicative of a magnetic phase transition. Three crystals were used with a total mass of 3.3 mg; a maximum is observed at 2.48 K, and a minimum at 4.91 K (inset of Fig. 8). The curve does not obey Debye's law or the T^3 law due to Schottky anomalies in the form of a lambda shape peak [22].

The heat capacity measurements as a function of temperature were measured at three different external magnetic fields. A decrease in the heat capacity maximum is seen at higher fields but no shift in the critical temperature is observed as in ferromagnetic materials [23].

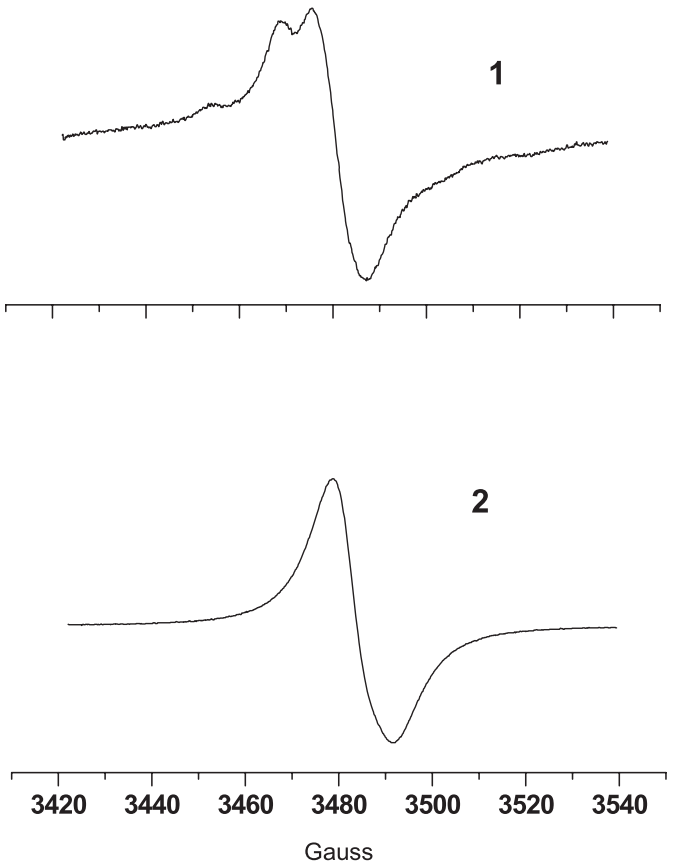

Fig. 5. EPR spectra in polycrystalline samples at room temperature for radicals **1** and **2**.

Conclusions

The presence of intramolecular hydrogen bonds results in different molecular symmetry; however, the two isomers show different crystal packing that leads to significantly different magnetic behavior. In radical **1** both ferro- and antiferromagnetic couplings compete, whereas in **2** only antiferromagnetic couplings are detected. Heat capacity measurements show a magnetic phase transition at T_c = 2.48 K for isomer **2**, higher than those observed in other nitronyl nitroxides.

Experimental

The two isomers were synthesized by reacting the corresponding aldehyde (Aldrich) with 2,3-bis(hydroxylamine) in methanol via oxidation with $NaIO_4$ in chloroform [24, 25].

2-(2'-hydroxyl-3'-methoxy-phenyl)-4, 4, 5, 5-tetramethyl-4, 5-dihydro-1H-imidazoyl-1-oxyl-3-oxide (1). Yield 61%, mp 150-151 ºC. IR (KBr) 3422(s), 2926(w), 1637(w), 1521(m), 1458(m), 1385(m), 1250(m), 1065(m), 789(m) cm^{-1}. UV (benzene) λ_{max} (log ε) 303 (4.07); 341 (3.98); 386 (3.71); 506 (2.87) nm. Anal. C 59.66, H 6.75, N 10.03, calcd for $C_{14}H_{19}N_2O_4$, C 60.20%, H 6.86%, N 10.03%, O 22.91%.

Table 2. *g*-values, hypertine splittings in solvents of differents polarity, and peak-to-peak bandwidths.

	$g^{\bullet}$	g°	$g^{\diamond}$	$a^{\bullet}$	$a^{\square}$	$a^{\diamond}$	$\Delta H_{pp}{}^{\bullet}$	$\Delta H_{pp}{}^{\square}$	$\Delta H_{pp}{}^{\diamond}$
1	2.0066	2.0066	2.0063	7.66	7.69	8.19	1.80	1.50	0.81
2	2.0067	2.0066	2.0063	7.49	7.66	8.12	2.13	1.42	1.11

•C_6H_6, □CH_2Cl_2, ◇H_2O. ΔHpp = Peak-to-peak bandwidth.

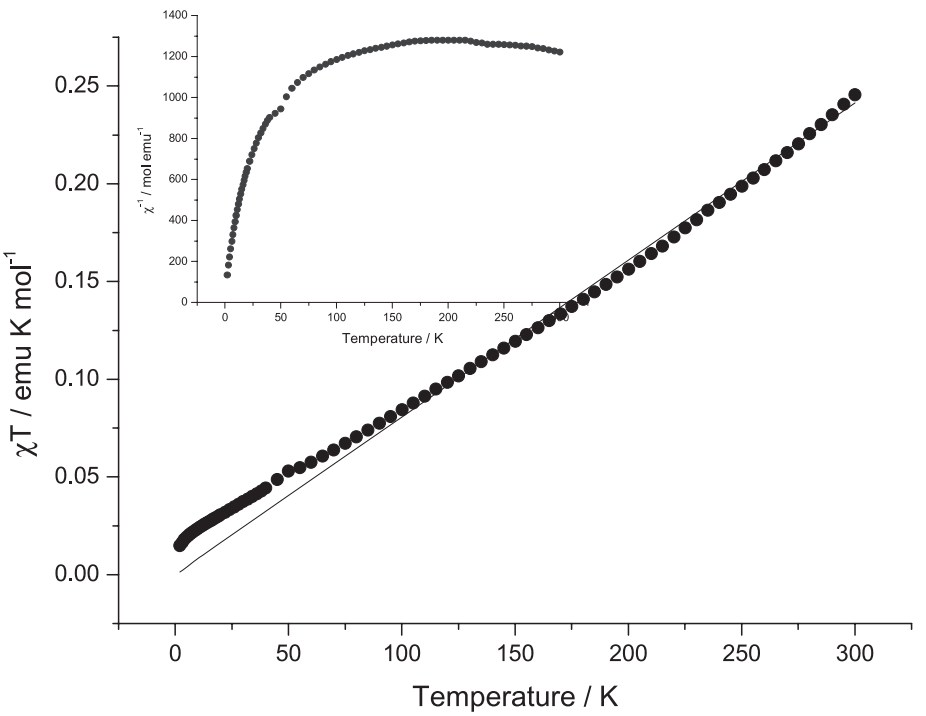

Fig. 6. Temperature dependence of χT for radical **1**. The solid line represents the best fit to the experimental data using the parameters J_F/k = + 0.11 K, J_{AF}/k = -0.81 K, zJ' = 0.013 K, g = 2.0067. Inset: Plot of the reciprocal magnetic susceptibility versus temperature.

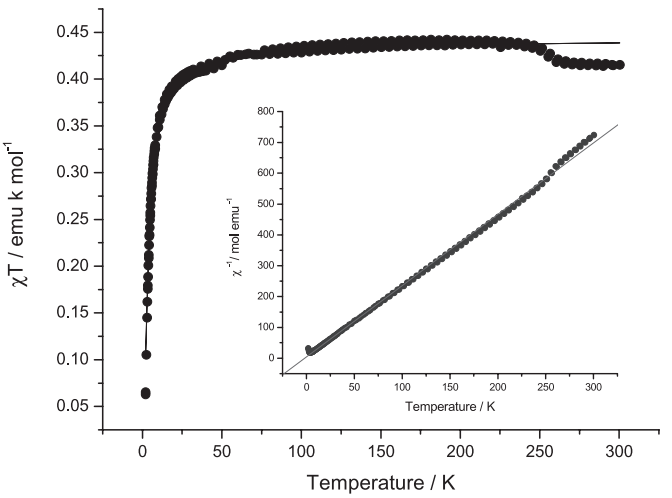

Fig. 7. Temperature dependence of χT for radical **2**. The solid line is the best fit to the experimental data using the parameters J_{AF}/k = - 1.60 and g = 2.0061. Inset: Plot of reciprocal magnetic susceptibility versus temperature.

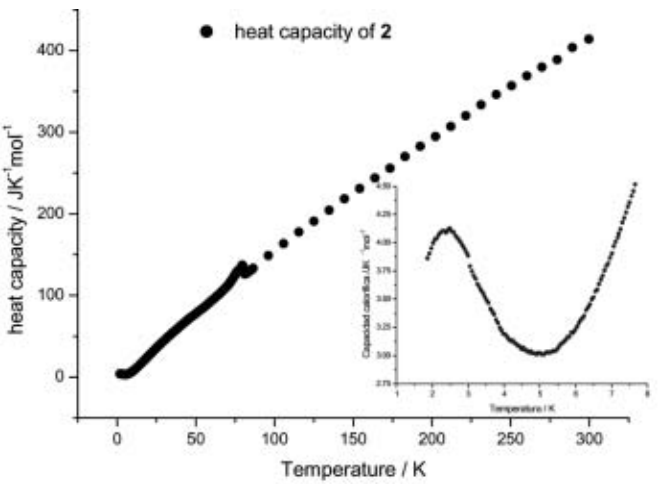

Fig. 8. Heat capacity as a function of temperature for radical **2**. Inset: Low temperature data showing the magnetic phase transition at the critical temperature 2.48 K.

2-(3'-hydroxyl-4'-methoxy-phenyl)-4, 4, 5, 5-tetramethyl-4, 5-dihydro-1H-imidazoyl-1-oxyl-3-oxide (2). Yield 17%, mp 90-91 ºC. IR (KBr) 3504(s), 2996(w), 1599(s), 1542(m), 1444(m), 1375(m), 1256(m), 1150(m), 768(m). UV (benzene) λ_{max} (log ε) 291 (3.96); 305 (3.76); 344 (3.54); 368 (3.72); 580 (2.32); 629 (2.36); 685 (2.31) nm. *Anal*. C 56.58, H 7.54, N 9.36, calcd for $C_{14}H_{21}N_2O_5$, C 56.55%, H 7.12%, N 9.42%.

Single crystals were grown at 0ºC from diethyl ether solutions. Crystals were mounted on glass fibers. The structures were solved by direct methods and refined by a full-matrix least-squares technique using the SHELX crystallographic software package [26] in the case of compound **1**, and Crystals2000 for compound **2** [27]. For radical **1** the intensities from X-ray diffraction were collected with a Bruker P4 XSCANS, release 2.21, with highly oriented crystalline graphite, and Mo-Kα radiation (λ = 0.71073 Å) at 300 K. Data were collected in the range $4.06 < 2\theta < 52^o$. For radical **2** an Enraf-Nonius CCD diffractometer was used with Mo-Kα radiation (λ = 0.71073 Å) at 293 K. Data were collected in the range $7.02 < 2\theta < 52.04^o$.

Supporting Information Available

The crystallographic data can be obtained free of charge via www.ccdc.cam.ac.uk/data_request/cif, or by emailing data_request@ccdc.cam.ac.uk, or by contacting The Cambridge Crystallographic Data Centre, 12, Union Road, Cambridge CB2 1EZ, UK; fax +44 1223 336033. CCDC 655342 contains the supplementary crystallographic data for compound **1**, and CCDC 655343 for compound **2**.

Acknowledgements

JP thanks Conacyt for financial support through project No. 400200-5-33564-E, and also to SEP for a PROMEP professorship. AV thanks Conacyt for scholarship No. 130434. We thank Dr. Francisco Morales for the magnetic measurements, and Dr. Roberto Escudero of the IIM-UNAM for the heat capacity measurements.

References

1. Tamura, M.; Nakazawa, Y.; Shiomi, D.; Nozawa, K.; Hosokoshi, Y.; Ishikawa, M.; Takahashi, M.; Kinoshita, M. *Chem. Phys. Lett*. **1991**, *186*, 401-404.
2. (a) Jeffrey, G. A., in: "An Introduction to Hydrogen Bonding", Topics in Physical Chemistry, Truhlar, D. G., Ed., Oxford University Press, London, **1997**, 98-103.
(b) Emsley, J., in: "Very Strong Hydrogen Bonding", *Chem. Soc. Rev.* **1980**, *9*, 91-124.
3. Hernández, E.; Mas, M.; Molins, E.; Rovira, C.; Veciana, J. *Angew. Chem. Int. Ed. Engl*. **1993**, *32*, 882-884.
4. Endtner, R.; Rentschler, E.; Bläser, D.; Boese, R.; Sutmann, R. *Eur. J. Org. Chem.* **2000**, 3347-3352.
5. Cirujeda, J.; Mas, M.; Molins, E.; Lanfranc de Panthou, F.; Laugier, J.; Paark, J. G.; Paulsen, C.; Rey, P.; Rovira, C.; Veciana, J. *J. Chem. Soc. Chem. Commun.* **1995**, 709-710.
6. Cirujeda, J.; Ochando, L. E.; Amigó, J. M.; Rovira, C.; Rius, J.; Veciana, J. *Angew. Chem. Int. Ed. Engl*. **1995**, *34*, 55-57.
7. Nakazawa, Y.; Tamura, M.; Shirakawa, N.; Shiomi, D.; Takahashi, M.; Kinoshita M.; Ishikawa, M. *Phys. Rev. B*, **1992**, *46*, 8906-8914.
8. Kinoshita, M.; Turek, P.; Tamura, M.; Nozawa, K.; Shiomi, D.; Nakazawa, Y.; Ishikama, M.; Takahashi, M.; Awaga, K.; Inabe, T.; Maruyama, Y. *Chem. Lett*. **1991**, 1225-1228.
9. Takahashi, M.; Turek, P.; Nakazawa, Y.; Tamura, M.; Nozawa, K.; Shiomi, D.; Ishikawa, M.; Kinoshita, M. *Phys. Rev. Lett*. **1991**, *67*, 746-748.
10. Matsushita, M. M.; Izuoka, A.; Sugawara, T.; Kobayashi, T.; Wada, N.; Takeda, N.; Ishikawa, M. *J. Am. Chem. Soc*. **1997**, *119*, 4369-4379.
11. Nakatsuji, S.; Morimoto, H.; Anzai, H.; Kawashima, J.; Maeda, K.; Mito, M.; Takeda, K. *Chem. Phys. Lett.* **1998**, *296*, 159-166.
12. Mito, M.; Deguchi, H.; Tamimoto, T.; Kawae, T.; Nakatsuji, S.; Morimoto, H.; Anzai, H.; Nakao, H.; Murakami, Y.; Takeda, K. *Phys. Rev. B* , **2003**, *67*, 024427/1-024427/8.
13. Yoshida, Y.; Tateiwa, N.; Mito, M.; Kawae, T.; Takeda, K.; Hosokoshi, Y.; Inoue, K. *Phys. Rev. Lett*. **2005**, *94*, 037203/1-037203/4.
14. Mito, M.; Kawae, T.; Hosokoshi, Y.; Inoue, K.; Kinoshita, M.; Takeda, K. *Solid State Commun*. **1999**, *111*, 607-611.
15. Hosokoshi, Y.; Tamura, M.; Kinoshita, M. *Mol. Cryst. and Liq. Cryst*. **1997**, *306*, 423-430.
16. Keana, J. F. W.; Norton, R. S.; Morello, M.; Van Engen D.; Clardy J, *J. Am. Chem. Soc*. **1978** *100*, 934-937.
17. Tretyakov, E.; Romanenko, G.; Podoplelov A.; Ovcharenko V, *Eur. J. Org. Chem*. **2006**, 2695-2702.
18. Awaga, K.; Maruyama, Y. *J. Chem. Phys*. **1989**, *91*, 2743-2747.
19. Sugano, T; Kurmoo, M; Uekusa, H; Ohashi, Y; Day, P. *J. Solid State Chem.* **1999**, *145*, 427-442.
20. Borrás-Almenar, J. J.; Coronado, E.; Curely, J.; Georges, R.; Gianduzzo, J. C. *Inorg. Chem.* **1994**, *33*, 5171-5175.
21. Bonner, J. C.; Fisher, M. E. *Phys. Rev.* **1964**, *135*, A640-A658.
22. Carlin, R. L. *Magnetochemistry*. Springer-Verlag, Berlin, **1986**.
23. Kinoshita, M. *Phil. Trans. R. Soc. Lond. A* **1999**, *357*, 2855-2872.
24. Hosokoshi, Y.; Tamura, M.; Sawa, H.; Kato, R.; Kinoshita, M. *J. Mater. Chem*. **1995**, *5*, 41-46.
25. Francese, G.; Romero, F. M.; Neels, A.; Stoeckli-Evans, H.; Decurtins, S. *Inorg. Chem.* **2000**, *39,* 2087-2095.
26. Sheldrick, G. M. *SHELX-97 Users Manual*, University of Göttingen, Germany. **1997**.
27. CRYSTALS2000. Betteridge, P. W.; Carruthers, J. R.; Cooper, R. I.; Prout, K.; Watkin, D. J. *J. Appl. Cryst.* **2003**, *36*, 1487-1487.